Analytical Formulation of Scattering From Anisotropic Power-Law Spectrum Surfaces: Getting Rid of the Cutoff Wavenumber

Gerardo Di Martino, *Senior Member, IEEE*, Alessio Di Simone, *Member, IEEE*, and Antonio Iodice, *Senior Member, IEEE*

***Abstract*— Sea and soil surfaces exhibit power-law spectra over a wide range of spatial frequencies. An analytical formulation of the electromagnetic scattering from such surfaces can be obtained via the two-scale model (TSM). However, this approach requires the definition of a cutoff surface wavenumber, separating the low- and high-frequency parts of the surface spectrum. The final obtained normalized radar cross section (NRCS) value is dependent on the choice of this cutoff wavenumber, which is, to some extent, arbitrary. This problem can be avoided by describing power-law spectrum surfaces via the theory of fractional Brownian motion (fBm) two-dimensional (2-D) random processes. The bistatic NRCS of an fBm surface can be analytically evaluated by using the Kirchhoff approximation (KA) or the first-order small slope approximation (SSA-1): its expression is related to the probability density function (pdf) of an alpha-stable random process, and it can be efficiently evaluated by means of proper asymptotic series expansions. However, fBm surfaces are statistically isotropic, whereas natural surfaces are often anisotropic. Therefore, in this work, we first of all show that an anisotropic power-law spectrum surface can be considered as a generalized anisotropic fBm surface; then, we present an analytical formulation of its NRCS, based on SSA-1; and finally, we compare the obtained results with measured NRCSs of natural surfaces and with NRCS values obtained via more accurate but more computationally demanding methods that require the numerical evaluation of scattering integrals.**

***Index Terms*— Anisotropic power-law spectrum surfaces, electromagnetic scattering, fractional Brownian motion (fBm), sea surface, small slope approximation (SSA).**

I. Introduction

ELECTROMAGNETIC scattering from natural rough surfaces is usually studied by modeling the surface roughness as a random process [1], [2], [3]. As it is by now widely recognized in literature, most marine and soil surfaces are well described by random processes, whose power spectral density (PSD), or spectrum, exhibits a power law behavior over a wide range of spatial frequencies [4], [5], [6], [7], usually including those involved in the microwave scattering phenomenon [7]. Therefore, it is of practical interest to evaluate the normalized radar cross section (NRCS) of power-law spectrum surfaces. To this aim, numerical methods, based on the method of moments (MoM) and Monte Carlo simulations, can be used; but, for extended two-dimensional (2-D) surfaces, their computational burden is too high for practical purposes. Therefore, approximate methods are usually preferred [1], [2], [3]. However, they often still require the numerical evaluation of scattering integrals. This can be avoided by using the two-scale model (TSM) [8], [9]: a cutoff surface wavenumber is selected, of the order of the incident electromagnetic wavenumber, and the overall surface NRCS is computed as the sum of the NRCSs of the high-frequency (or small-scale) roughness (i.e., the surface spatial-frequency components at wavenumbers higher than the cutoff one) and of the low-frequency (or large-scale) roughness (i.e., the surface spatial-frequency components at wavenumbers lower than the cutoff one). The former is computed by using the small perturbation method (SPM) [1], [2], [3], and it is dominant at far-from-specular scattering directions, while the latter is computed by using the geometrical optics (GO) approximation [1], [2], [3], and it is dominant at near-specular scattering directions. With this approach, that can be applied to both isotropic and anisotropic power-law spectrum surfaces, a fairly simple analytical expression of the NRCS is obtained (if the SPM NRCS is not averaged over the large-scale slopes, or this average is approximated [10]). However, this expression depends on the choice of the cutoff wavenumber, which is to some extent arbitrary: this is the main drawback of the TSM.

A different analytical approach that avoids both the numerical evaluation of the scattering integral and the necessity of defining a cutoff wavenumber was provided in [7], [11], [12], [13], and [14]: by describing statistically isotropic power-law spectrum surfaces via the theory of 2-D fractional Brownian motion (fBm) random processes [4], [5], it was shown that the scattering integral appearing in their NRCS, as computed via the Kirchhoff approximation (KA) [1], [2], [3], is formally identical to the probability density function (pdf) of an alpha-stable random process [14], and it can be efficiently evaluated by means of proper asymptotic series expansions [7], [12], [13]. The fact that the KA scattering integral of a power-law spectrum surface is formally identical to the pdf of an alpha-stable random process was also shown in [15]

Manuscript received 25 July 2023; revised 14 September 2023; accepted 16 October 2023. Date of publication 18 October 2023; date of current version 2 November 2023. This study was carried out within the Agritech National Research Center and received funding from the European Union Next-GenerationEU (PIANO NAZIONALE DI RIPRESA E RESILIENZA (PNRR) – MISSIONE 4 COMPONENTE 2, INVESTIMENTO 1.4 – D.D. 1032 17/06/2022, CN00000022). This manuscript reflects only the authors' views and opinions, neither the European Union nor the European Commission can be considered responsible for them. *(Corresponding author: Antonio Iodice.)*

The authors are with the Department of Electrical Engineering and Information Technology, University of Naples Federico II, 80125 Naples, Italy (e-mail: gerardo.dimartino@unina.it; alessio.disimone@unina.it; iodice@unina.it).

Digital Object Identifier 10.1109/TGRS.2023.3325722

by using the theory of infinite-variance random processes, but there an analytical solution was only provided in the high-frequency limit.

Since the same scattering integral also appears in the NRCS expression obtained by using the first-order small slope approximation (SSA-1) [16], [17], the method of [7], [11], [12], [13], and [14] can also be applied in the framework of the SSA-1, which has a wider range of validity with respect to KA. This was first noticed in [14] and has been recently fully implemented in [18].

In any case, since 2-D fBm processes are statistically isotropic, this method can be only applied to statistically isotropic power-law spectrum surfaces. However, natural surfaces are often statistically anisotropic due to the presence of a surface preferential direction: this is the case of marine surfaces, for which the preferential direction is the wind direction, and of tilled soil surfaces, for which the preferential direction is the plowing direction. Therefore, in this article, we extend the method of [7], [11], [12], [13], and [14] to the case of statistically anisotropic power-law spectrum surfaces. To this aim, we first show that the latter can be considered as generalized anisotropic fBm surfaces; then, we provide an analytical formulation of their NRCS by using the SSA-1; finally, we compare the obtained results with measured NRCSs of natural surfaces and with NRCS values obtained via more refined but more computationally demanding methods that require the numerical evaluation of scattering integrals.

II. Anisotropic Power-Law Spectrum Surface

Let us consider a rough surface $z(x, y)$ separating the air from a possibly lossy medium and illuminated by an incident electromagnetic wave with incidence angle $\vartheta_i \vartheta_{\mathrm{i}}$. The xy plane is the surface mean plane, and the xz plane is the incidence plane (see Fig. 1). Let us assume that $z(x, y)$ is a zero-mean Gaussian random process, whose PSD is

$$S_{2\mathrm{D}}(\kappa_x, \kappa_y) = S_{2\mathrm{D}}(\kappa, \varphi) = S(\kappa)\Phi(\varphi) \tag{1}$$

with

$$S(\kappa) = S_0 \kappa^{-\alpha} \tag{2}$$

and

$$\Phi(\varphi) = 1 + \Delta \cos[2(\varphi - \varphi_0)] \tag{3}$$

where κ and φ indicate the amplitude and direction of the surface wavenumber vector, and κ_x and κ_y are its x and y components, with

$$\begin{cases} \kappa_x = \kappa \cos\varphi \\ \kappa_y = \kappa \sin\varphi, \end{cases} \quad \text{i.e.,} \quad \begin{cases} \kappa = \sqrt{\kappa_x^2 + \kappa_y^2} \\ \tan\varphi = \kappa_y/\kappa_x. \end{cases} \tag{4}$$

S_0 is a parameter measured in $\mathrm{m}^{4-\alpha}$, α is the power exponent, satisfying $2 < \alpha < 4$, Δ is the spectral anisotropy parameter, satisfying $0 \le \Delta < 1$, and φ_0 is the angle between the x-axis and the X-axis of the preferential reference system X–Y of the anisotropic surface (for instance, for a sea surface, X and Y axes are the upwind and crosswind directions, respectively, and φ_0 stands for the wind direction).

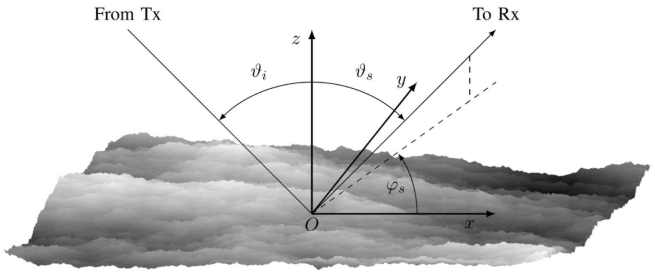

Fig. 1. Geometry of the problem.

The above defined process has infinite variance, it is statistically anisotropic and nonstationary, and its derivatives have infinite variance, too. However, it is a stationary-increment process [19], so that it is possible to define its structure function $Q_{2\mathrm{D}}(\Delta x, \Delta y)$ as the variance of its increments over two generic points displaced by Δx and Δy over x- and y-axes, respectively

$$Q_{2\mathrm{D}}(\Delta x, \Delta y) = \langle |z(x+\Delta x, y+\Delta y) - z(x, y)|^2 \rangle \tag{5}$$

where the symbol $\langle \cdot \rangle$ stands for statistical mean.

The structure function is related to the PSD via the following relation [19]:

$$Q_{2\mathrm{D}}(\Delta x, \Delta y) = \frac{1}{4\pi^2} \int_{-\infty}^{+\infty} \int_{-\infty}^{+\infty} 2\left[1 - \mathrm{e}^{j(\kappa_x \Delta x + \kappa_y \Delta y)}\right] \times S_{2\mathrm{D}}(\kappa_x, \kappa_y)\, \mathrm{d}\kappa_x \mathrm{d}\kappa_y. \tag{6}$$

We will now exploit this relation to evaluate the structure function of the anisotropic power-law spectrum surface of (1)–(4).

By using (1)–(4) in (6) and letting

$$\begin{cases} \Delta x = \rho \cos\psi \\ \Delta y = \rho \sin\psi, \end{cases} \quad \text{i.e.,} \quad \begin{cases} \rho = \sqrt{\Delta x^2 + \Delta y^2} \\ \tan\psi = \Delta y/\Delta x \end{cases} \tag{7}$$

where ρ and ψ indicate the length and direction of the segment joining the two surface points, and we get

$$\begin{aligned} &Q_{2\mathrm{D}}(\Delta x, \Delta y) \\ &\quad = Q_{2\mathrm{D}}(\rho, \psi) \\ &\quad = \frac{1}{4\pi^2} \int_0^{\infty} \int_0^{2\pi} 2\left[1 - \mathrm{e}^{j\kappa\rho\cos(\varphi-\psi)}\right] S(\kappa)\Phi(\varphi)\kappa\, \mathrm{d}\varphi \mathrm{d}\kappa \\ &\quad = \frac{S_0}{2\pi^2} \int_0^{\infty} \kappa^{-\alpha+1} \int_0^{2\pi} \left[1 - \mathrm{e}^{j\kappa\rho\cos(\varphi-\psi)}\right] \Phi(\varphi)\, \mathrm{d}\varphi \mathrm{d}\kappa. \end{aligned} \tag{8}$$

By letting $\bar{\kappa} = \kappa\rho$, we obtain

$$\begin{aligned} &Q_{2\mathrm{D}}(\rho, \psi) \\ &= \rho^{\alpha-2} \frac{S_0}{2\pi^2} \int_0^{\infty} \bar{\kappa}^{-\alpha+1} \int_0^{2\pi} \left[1 - \mathrm{e}^{j\bar{\kappa}\cos(\varphi-\psi)}\right] \Phi(\varphi)\, \mathrm{d}\varphi \mathrm{d}\bar{\kappa} \\ &= \rho^{2H} \frac{S_0}{\pi} \int_0^{\infty} \bar{\kappa}^{-1-2H} \left\{1 - J_0(\bar{\kappa}) + \Delta J_2(\bar{\kappa}) \cos[2(\psi - \varphi_0)]\right\} \mathrm{d}\bar{\kappa} \end{aligned} \tag{9}$$

where

$$J_0(\bar{\kappa}) = \frac{1}{2\pi} \int_0^{2\pi} \mathrm{e}^{j\bar{\kappa}\cos(\varphi-\psi)} \mathrm{d}\varphi \tag{10}$$

is the zeroth-order Bessel function of the first kind [20], and $J_2(\bar{\kappa})$ is the second-order Bessel function of the first kind, for which, see Appendix A, the following equality holds:

$$\int_0^{2\pi} e^{j\bar{\kappa}\cos(\varphi-\psi)}\cos[2(\varphi-\varphi_0)]d\varphi = -2\pi J_2(\bar{\kappa})\cos[2(\psi-\varphi_0)] \quad (11)$$

and, finally, we have set $\alpha - 2 = 2H$, so that $\alpha = 2 + 2H$ and $0 < H < 1$.

By using integration by parts, it turns out that

$$\int_0^{\infty} \bar{\kappa}^{-1-2H}\{1-J_0(\bar{\kappa})\}d\bar{\kappa} = \frac{1}{2H}\int_0^{\infty}\bar{\kappa}^{-2H}J_1(\bar{\kappa})d\bar{\kappa} = \frac{\Gamma(1-H)}{2H2^{2H}\Gamma(1+H)} \quad (12)$$

where $J_1(\bar{\kappa})$ is the first-order Bessel function of the first kind, that is the derivative of $-J_0(\bar{\kappa})$, $\Gamma(\cdot)$ is the gamma function, and the following equality [21]:

$$\int_0^{\infty} z^{\mu}J_{\nu}(z)dz = \frac{2^{\mu}\Gamma\left(\frac{1+\nu+\mu}{2}\right)}{\Gamma\left(\frac{1+\nu-\mu}{2}\right)} \quad (13)$$

that holds for $\mu < 1/2$ and $\mu + \nu > -1$ has been used with $\mu = -2H$ and $\nu = 1$.

By using the same equality, but with $\mu = -1 - 2H$ and $\nu = 2$, we get

$$\int_0^{\infty}\bar{\kappa}^{-1-2H}J_2(\bar{\kappa})d\bar{\kappa} = \frac{\Gamma(1-H)}{2^{1+2H}\Gamma(2+H)} = \frac{\Gamma(1-H)}{2^{1+2H}(1+H)\Gamma(1+H)}. \quad (14)$$

By replacing (12) and (14) in (9), we finally get

$$Q_{2D}(\rho,\psi) = \rho^{2H}\frac{S_0\Gamma(1-H)}{2\pi H2^{2H}\Gamma(1+H)}\left\{1+\frac{H}{1+H}\Delta\cos[2(\psi-\varphi_0)]\right\} = Q(\rho)\Psi(\psi) \quad (15)$$

where

$$Q(\rho) = s^2\rho^{2H} \quad (16)$$

and

$$\Psi(\psi) = \{1+\delta\cos[2(\psi-\varphi_0)]\} \quad (17)$$

with

$$s^2 = \frac{S_0\Gamma(1-H)}{2\pi H2^{2H}\Gamma(1+H)} \quad (18)$$

and

$$\delta = \frac{H}{1+H}\Delta \quad (19)$$

so that $0 \le \delta < H/(1+H)$. We explicitly note that s^2 is measured in $m^{4-\alpha}$, i.e., m^{2-2H}.

The result of (15)–(19) is new and it generalizes to the anisotropic case the known analogous result for the isotropic case [12], [22], to which it reduces for $\Delta = 0$.

We recall that an fBm is a process whose increments over a fixed distance ρ are zero-mean Gaussian random variables with variance proportional to ρ^{2H} [4], [5]. Therefore, (15)–(19) show that if $\Delta = 0$ (isotropic case), the considered power-law surface is a 2-D fBm, as already known. For $\Delta > 0$, (15)–(19) show that any height profile obtained from a cut of the considered power-law surface along an arbitrary direction is a 1-D fBm. Therefore, for $\Delta > 0$, the anisotropic power-law spectrum surface defined in (1)–(4) can be considered as the anisotropic generalization of an fBm surface.

The variance of such a surface is infinite; however, the measured variance σ_{ψ}^2 of the height of one of its profiles of length l along a direction ψ is finite and increases with l

$$\sigma_{\psi}^2(l) \sim \frac{1}{2}Q(l)\Psi(\psi) = \frac{1}{2}s^2l^{2H}\Psi(\psi). \quad (20)$$

Average over all directions (i.e., over ψ) leads to the following measured variance σ^2 of the height of a surface patch of linear size l:

$$\sigma^2(l) \sim \frac{1}{2}s^2l^{2H}. \quad (21)$$

Similarly, the variance of the slopes of an anisotropic fBm process is infinite; however, the variance of slopes measured at a scale ρ along a direction ψ (i.e., the variance of slopes of chords joining surface points at a fixed distance ρ along a direction ψ) is finite and increases as ρ decreases

$$\sigma_{s\psi}^2(\rho) = Q(\rho)\Psi(\psi)/\rho^2 = s^2\Psi(\psi)/\rho^{2-2H}. \quad (22)$$

III. Normalized Radar Cross Section

Let us consider a surface satisfying (1)–(4) in a wide but limited range of spatial wavenumbers, from $\kappa_{\min}$ to $\kappa_{\max}$, with $\kappa_{\min} \ll \kappa_{\max}$. It will also satisfy (15)–(19) in a wide but limited range of scales, from $\rho_{\min} \sim 2\pi/\kappa_{\max}$ to $\rho_{\max} \sim 2\pi/\kappa_{\min}$. Let us also assume that this range of scales includes those involved in the microwave scattering phenomenon, so that the formulation of (15)–(19) can be used to model the surface in electromagnetic scattering problems. In Section IV, we will show that many natural surfaces satisfy these hypotheses.

A. General Expression of the NRCS

The SSA-1 expression of the NRCS of a randomly rough surface is [16], [17]

$$\sigma_{pq}^0(\vartheta_i;\vartheta_s,\varphi_s) = \frac{1}{\pi}\left|\frac{2kvB_{pq}}{u_z}\right|^2\int_{-\infty}^{+\infty}\int_{-\infty}^{+\infty}e^{-jk(u_x\Delta x+u_y\Delta y)} \times e^{-\frac{1}{2}k^2u_z^2Q_{2D}(\Delta x,\Delta y)}d\Delta x d\Delta y \quad (23)$$

where (see Fig. 1) ϑ_i is the incidence angle, ϑ_s and φ_s are the polar and azimuthal scattering angles, $k = 2\pi/\lambda$ is the electromagnetic wavenumber, λ is the electromagnetic wavelength, and $v = \cos\vartheta_s\cos\vartheta_i$

$$\begin{cases} u_x = \sin\vartheta_i - \sin\vartheta_s\cos\varphi_s \\ u_y = -\sin\vartheta_s\sin\varphi_s \\ u_z = -(\cos\vartheta_i + \cos\vartheta_s) \end{cases} \quad (24)$$

and as in (25), shown at the bottom of the next page, are the bistatic Bragg coefficients, with ε being the relative

permittivity of the lower medium. Finally, p and q may each stand for horizontal (h) or vertical (v) polarization.

Note that $\kappa_{Bx} = ku_x$ and $\kappa_{By} = ku_y$ are the x and y components of the surface Bragg wavenumber vector.

By using (7) and (15)–(19) in (23), and letting

$$\begin{cases} u_x = u_\rho \cos\varphi_B \\ u_y = u_\rho \sin\varphi_B, \end{cases} \quad \text{i.e.,} \quad \begin{cases} u_\rho = \sqrt{u_x^2 + u_y^2} \\ \tan\varphi_B = u_y/u_x \end{cases} \tag{26}$$

we get

$$\sigma^0_{pq}(\vartheta_i;\vartheta_s,\varphi_s) = \frac{1}{\pi}\left|\frac{2kvB_{pq}}{u_z}\right|^2 \int_0^{2\pi}\int_0^{\infty} \mathrm{e}^{-jku_\rho\rho\cos(\varphi_B-\psi)} \times \mathrm{e}^{-\frac{1}{2}k^2u_z^2s^2\Psi(\psi)\rho^{2H}} \rho d\rho d\psi. \tag{27}$$

We assume that the linear size l of the illuminated surface patch is such that $k^2u_z^2s^2l^{2H} \gg 1$, so that the integral in (27) can span the entire real plane, since the integrand is negligible outside the illuminated area.

If $\delta \ll 1$ (in practice, it is sufficient that $\delta < 0.2$), the second exponential in (27) can be written as

$$\begin{aligned} &\mathrm{e}^{-\frac{1}{2}k^2u_z^2s^2\Psi(\psi)\rho^{2H}} \\ &\quad = \mathrm{e}^{-\frac{1}{2}k^2u_z^2s^2\rho^{2H}} \mathrm{e}^{-\frac{1}{2}k^2u_z^2s^2\delta\cos[2(\psi-\varphi_0)]\rho^{2H}} \\ &\quad \cong \mathrm{e}^{-\frac{1}{2}k^2u_z^2s^2\rho^{2H}} \left\{1-\frac{1}{2}k^2u_z^2s^2\delta\cos[2(\psi-\varphi_0)]\rho^{2H}\right\} \end{aligned} \tag{28}$$

so that (27) can be rewritten as

$$\begin{aligned} &\sigma^0_{pq}(\vartheta_i;\vartheta_s,\varphi_s) \\ &\quad = \frac{1}{\pi}\left|\frac{2kvB_{pq}}{u_z}\right|^2 \int_0^{\infty} \mathrm{e}^{-\frac{1}{2}k^2u_z^2s^2\rho^{2H}} \int_0^{2\pi} \mathrm{e}^{-jku_\rho\rho\cos(\varphi_B-\psi)} \\ &\qquad \times\left\{1-\frac{1}{2}k^2u_z^2s^2\delta\cos[2(\psi-\varphi_0)]\rho^{2H}\right\} d\psi\rho d\rho. \end{aligned} \tag{29}$$

By using (10) and (11), with the obvious formal modifications, to evaluate the integral over ψ in (29), we obtain

$$\begin{aligned} &\sigma^0_{pq}(\vartheta_i;\vartheta_s,\varphi_s) \\ &\quad = 2\left|\frac{2kvB_{pq}}{u_z}\right|^2 \left\{\int_0^{\infty} J_0(ku_\rho\rho)\mathrm{e}^{-\frac{1}{2}k^2u_z^2s^2\rho^{2H}}\rho d\rho \right. \\ &\qquad + \frac{1}{2}k^2u_z^2s^2\delta\cos[2(\varphi_B-\varphi_0)] \\ &\qquad \left. \times \int_0^{\infty} J_2(ku_\rho\rho)\mathrm{e}^{-\frac{1}{2}k^2u_z^2s^2\rho^{2H}}\rho^{1+2H}d\rho\right\}. \end{aligned} \tag{30}$$

In Appendixes B and C, we show that the integrals in (30) can be analytically evaluated via asymptotic series. In particular, for small values of the dimensionless parameter

$$\Omega = \frac{\frac{1}{2}k^2u_z^2s^2}{\left(k^2u_\rho^2\right)^H} = \frac{1}{2}s^2k^{2-2H}\frac{u_z^2}{u_\rho^{2H}} \tag{31}$$

the following asymptotic series expansion is obtained (see Appendix B):

$$\begin{aligned} &\sigma^0_{pq}(\vartheta_i;\vartheta_s,\varphi_s) \\ &\quad = 2\left|\frac{2kvB_{pq}}{u_z}\right|^2 2H\sum_{n=1}^{\infty}\frac{(-1)^{n+1}2^{2nH}}{n!}\frac{n\Gamma(1+nH)}{\Gamma(1-nH)}\frac{\left(\frac{1}{2}k^2u_z^2s^2\right)^n}{\left(k^2u_\rho^2\right)^{1+nH}} \\ &\qquad \times\left\{1+\frac{1+nH}{H}\delta\cos[2(\varphi_B-\varphi_0)]\right\}. \end{aligned} \tag{32}$$

Conversely, for large values of Ω, the following asymptotic series expansion is obtained (see Appendix C):

$$\begin{aligned} &\sigma^0_{pq}(\vartheta_i;\vartheta_s,\varphi_s) \\ &\quad = 2\left|\frac{2kvB_{pq}}{u_z}\right|^2 \frac{1}{2H}\sum_{n=0}^{\infty}\frac{(-1)^n}{2^{2n}(n!)^2}\Gamma\left(\frac{n+1}{H}\right)\frac{k^{2n}u_\rho^{2n}}{\left(\frac{1}{2}k^2u_z^2s^2\right)^{\frac{n+1}{H}}} \\ &\qquad \times\left\{1-\frac{n}{H}\delta\cos[2(\varphi_B-\varphi_0)]\right\}. \end{aligned} \tag{33}$$

Some practical details about the evaluation of the bistatic NRCS according to (32) and (33) are provided in the following (see the discussion on computational complexity in Section IV-B).

B. Limiting Cases

Equations (32) and (33) generalize to the anisotropic case results of [7], [12], [13], and [14], and they reduce to them for $\delta = 0$. They are the main results of our work, and in Section IV, we will show that they allow to efficiently compute the NRCS of anisotropic natural surfaces. However, it is interesting to consider the limiting cases of either very small or very large values of the parameter Ω. In fact, this parameter can be written as

$$\Omega = \frac{\frac{1}{2}k^2u_z^2s^2}{\kappa_B^{2H}} = k^2u_z^2\frac{1}{2}s^2\left(\frac{\Lambda_B}{2\pi}\right)^{2H} = k^2u_z^2\sigma^2\left(\frac{\Lambda_B}{2\pi}\right) \tag{34}$$

where $\kappa_B = ku_\rho$ and $\Lambda_B = 2\pi/\kappa_B$ are the surface Bragg resonant wavenumber and wavelength, respectively, and (21)

$$\begin{cases} B_{hh} = \dfrac{(\varepsilon-1)\cos\varphi_s}{\left(\cos\vartheta_s+\sqrt{\varepsilon-\sin^2\vartheta_s}\right)\left(\cos\vartheta_i+\sqrt{\varepsilon-\sin^2\vartheta_i}\right)} \\ B_{vh} = \dfrac{\sin\varphi_s(\varepsilon-1)\sqrt{\varepsilon-\sin^2\vartheta_s}}{\left(\varepsilon\cos\vartheta_s+\sqrt{\varepsilon-\sin^2\vartheta_s}\right)\left(\cos\vartheta_i+\sqrt{\varepsilon-\sin^2\vartheta_i}\right)} \\ B_{hv} = \dfrac{\sin\varphi_s(\varepsilon-1)\sqrt{\varepsilon-\sin^2\vartheta_i}}{\left(\cos\vartheta_s+\sqrt{\varepsilon-\sin^2\vartheta_s}\right)\left(\varepsilon\cos\vartheta_i+\sqrt{\varepsilon-\sin^2\vartheta_i}\right)} \\ B_{vv} = \dfrac{(\varepsilon-1)\left(\sqrt{\varepsilon-\sin^2\vartheta_s}\sqrt{\varepsilon-\sin^2\vartheta_i}\cos\varphi_s-\varepsilon\sin\vartheta_s\sin\vartheta_i\right)}{\left(\varepsilon\cos\vartheta_s+\sqrt{\varepsilon-\sin^2\vartheta_s}\right)\left(\varepsilon\cos\vartheta_i+\sqrt{\varepsilon-\sin^2\vartheta_i}\right)} \end{cases} \tag{25}$$

has been used. Therefore, Ω is the Rayleigh parameter for surface patches of linear size of the order of the Bragg wavelength. In Appendix B, we show that for small Ω, the scale lengths involved in the scattering phenomenon are just those around the Bragg wavelength. Therefore, if Ω is small, then Ω is the Rayleigh parameter for surface patches of linear size of the order of the scale lengths actually involved in the scattering phenomenon.

For $\Omega \ll 1$, the terms in (32) with $n > 1$ are negligible, and the series can be truncated at the first order, so obtaining

$$\sigma^0_{pq}(\vartheta_i;\vartheta_s,\varphi_s) \cong 4k^4v^2\left|B_{pq}\right|^2\frac{2H2^{2H}\Gamma(1+H)}{\Gamma(1-H)}\frac{s^2}{\left(ku_\rho\right)^{2+2H}} \times\left\{1+\frac{1+H}{H}\delta\cos[2(\varphi_B-\varphi_0)]\right\}. \tag{35}$$

By using (18) and (19) in (35), we get

$$\sigma^0_{pq}(\vartheta_i;\vartheta_s,\varphi_s) \cong \frac{4}{\pi}k^4v^2\left|B_{pq}\right|^2S_0\left(ku_\rho\right)^{-\alpha}\{1+\Delta\cos[2(\varphi_B-\varphi_0)]\} \tag{36}$$

i.e., see (15)–(17)

$$\sigma^0_{pq}(\vartheta_i;\vartheta_s,\varphi_s) = \frac{4}{\pi}k^4v^2\left|B_{pq}\right|^2S_{2D}\left(ku_\rho,\varphi_B\right) = \frac{4}{\pi}k^4v^2\left|B_{pq}\right|^2S_{2D}\left(\kappa_{Bx},\kappa_{By}\right) \tag{37}$$

which is coincident with the SPM formulation of the NRCS, as expected for very small values of the Rayleigh parameter.

Let us now consider the case $\Omega \gg 1$, which is always satisfied at near-specular direction, where $\vartheta_s \cong \vartheta_i$ and $\varphi_s \cong 0$, so that $u_\rho \cong 0$. In this case, the terms in (33) with $n > 1$ are negligible, and the series can be truncated at the first order (i.e., considering only the terms with $n = 0$ and $n = 1$), so obtaining

$$\begin{aligned}\sigma^0_{pq}(\vartheta_i;\vartheta_s,\varphi_s) &\cong 2\left|\frac{2kvB_{pq}}{u_z}\right|^2\frac{\Gamma(1/H)}{2H\left(\frac{1}{2}k^2s^2u_z^2\right)^{1/H}} \times\left(1-\frac{\Gamma(2/H)k^2u_\rho^2\left\{1-\frac{1}{H}\delta\cos[2(\varphi_B-\varphi_0)]\right\}}{4\Gamma(1/H)\left(\frac{1}{2}k^2s^2u_z^2\right)^{1/H}}\right)\\ &\cong 2\left|\frac{2kvB_{pq}}{u_z}\right|^2\frac{\Gamma(1/H)}{2H\left(\frac{1}{2}k^2s^2u_z^2\right)^{1/H}} \times\exp\left(-\frac{\Gamma(2/H)k^2u_\rho^2\left\{1-\frac{1}{H}\delta\cos[2(\varphi_B-\varphi_0)]\right\}}{4\Gamma(1/H)\left(\frac{1}{2}k^2s^2u_z^2\right)^{1/H}}\right).\end{aligned} \tag{38}$$

This expression can be reformulated in terms of the anisotropic fBm surface slope variances along X- and Y-directions as measured at the scale length mainly involved in the scattering phenomenon, that for large Ω, as shown in Appendix C, is

$$\rho_0 = \frac{1}{\left[\frac{1}{2}k^2s^2\Psi(\psi)u_z^2\right]^{\frac{1}{2H}}}. \tag{39}$$

In fact, by using (22) and (39) with $\psi = \varphi_0$ (for the X-direction) and with $\psi = \varphi_0 + \pi/2$ (for the Y-direction), and recalling that $\delta \ll 1$, we get

$$\sigma^2_{sX,Y}(\rho_0) = \frac{s^2(1\pm\delta)}{\rho_0^{2-2H}} = \frac{\left[\frac{1}{2}k^2s^2(1\pm\delta)u_z^2\right]^{\frac{1}{H}}}{\frac{1}{2}k^2u_z^2} \cong \frac{\left[\frac{1}{2}k^2s^2u_z^2\right]^{\frac{1}{H}}(1\pm\frac{\delta}{H})}{\frac{1}{2}k^2u_z^2} \tag{40}$$

so that

$$\frac{\sigma^2_{sX}(\rho_0)+\sigma^2_{sY}(\rho_0)}{2} \cong \frac{\left[\frac{1}{2}k^2s^2u_z^2\right]^{\frac{1}{H}}}{\frac{1}{2}k^2u_z^2} \cong \sigma_{sX}(\rho_0)\sigma_{sY}(\rho_0) \tag{41}$$

and

$$\frac{\sigma^2_{sX}(\rho_0)-\sigma^2_{sY}(\rho_0)}{2} \cong \frac{\left[\frac{1}{2}k^2s^2u_z^2\right]^{\frac{1}{H}}}{\frac{1}{2}k^2u_z^2}\frac{\delta}{H}. \tag{42}$$

By using (41) and (42), the expression in (38) can be reformulated as

$$\begin{aligned}&\sigma^0_{pq}(\vartheta_i;\vartheta_s,\varphi_s)\\ &= \frac{8\left|B_{pq}\right|^2v^2\Gamma(1/H)}{Hu_z^4\sigma_{sX}(\rho_0)\sigma_{sY}(\rho_0)} \times\exp\left(-\frac{\Gamma(2/H)u_\rho^2\left\{1-\frac{\sigma^2_{sX}(\rho_0)-\sigma^2_{sY}(\rho_0)}{\sigma^2_{sX}(\rho_0)+\sigma^2_{sY}(\rho_0)}\cos[2(\varphi_B-\varphi_0)]\right\}}{2u_z^2\Gamma(1/H)\sigma_{sX}(\rho_0)\sigma_{sY}(\rho_0)}\right)\\ &= \frac{a8\left|B_{pq}\right|^2v^2}{u_z^4\sigma_{sX\text{eff}}\sigma_{sY\text{eff}}} \times\exp\left(-\frac{u_\rho^2\left\{1-\frac{\sigma^2_{sX\text{eff}}-\sigma^2_{sY\text{eff}}}{\sigma^2_{sX\text{eff}}+\sigma^2_{sY\text{eff}}}\cos[2(\varphi_B-\varphi_0)]\right\}}{2u_z^2\sigma_{sX\text{eff}}\sigma_{sY\text{eff}}}\right)\end{aligned} \tag{43}$$

where

$$\sigma^2_{sX,Y\text{eff}} = b\sigma^2_{sX,Y}(\rho_0), \quad a = \frac{\Gamma^2(1/H)}{H\Gamma(2/H)}, \quad b = \frac{\Gamma(1/H)}{\Gamma(2/H)} \tag{44}$$

with a and b being of the order of unity for $H > 0.5$, which is the case for most natural surfaces, as we will see in Section IV.

It is interesting to compare this expression with the usual GO expression of the NRCS [1], [2], [3], [10], [23], [24] that at near specular direction can be written as

$$\sigma^0_{pq}(\vartheta_i;\vartheta_s,\varphi_s) = \frac{8\left|B_{pq}\right|^2v^2}{u_z^4\sigma_{sX}\sigma_{sY}}\mathrm{e}^{-\frac{\sigma^2_{sx}u_x^2+\sigma^2_{sy}u_y^2-2\mathrm{corr}_{sxy}u_xu_y}{2u_z^2\sigma^2_{sX}\sigma^2_{sY}}} \tag{45}$$

where $\sigma^2_{sX}, \sigma^2_{sY}, \sigma^2_{sx}$, and σ^2_{sy} are the slope variances along the directions X, Y, x, and y, respectively, and corr_{sxy} is the correlation between the slopes along x- and y-directions.

By using (26) and the following relations [10]:

$$\begin{cases}\sigma^2_{sx} = \sigma^2_{sX}\cos^2\varphi_0 + \sigma^2_{sY}\sin^2\varphi_0\\ \sigma^2_{sy} = \sigma^2_{sY}\cos^2\varphi_0 + \sigma^2_{sX}\sin^2\varphi_0\\ \mathrm{corr}_{sxy} = \frac{1}{2}\sin 2\varphi_0\left(\sigma^2_{sX}-\sigma^2_{sY}\right)\end{cases} \tag{46}$$

after some algebra, (45) can be recast as follows:

$$\sigma^0_{pq}(\vartheta_i;\vartheta_s,\varphi_s) = \frac{8\left|B_{pq}\right|^2 v^2}{u_z^4\sigma_{sX}\sigma_{sY}}\exp\left(-\frac{u_\rho^2\frac{\sigma_{sX}^2+\sigma_{sY}^2}{2}\left\{1-\frac{\sigma_{sX}^2-\sigma_{sY}^2}{\sigma_{sX}^2+\sigma_{sY}^2}\cos[2(\varphi_B-\varphi_0)]\right\}}{2u_z^2\sigma_{sX}^2\sigma_{sY}^2}\right) \cong \frac{8\left|B_{pq}\right|^2 v^2}{u_z^4\sigma_{sX}\sigma_{sY}}\exp\left(-\frac{u_\rho^2\left\{1-\frac{\sigma_{sX}^2-\sigma_{sY}^2}{\sigma_{sX}^2+\sigma_{sY}^2}\cos[2(\varphi_B-\varphi_0)]\right\}}{2u_z^2\sigma_{sX}\sigma_{sY}}\right) \tag{47}$$

where the last approximate equality holds for $(\sigma_{sX}^2-\sigma_{sY}^2)/(\sigma_{sX}^2+\sigma_{sY}^2)\ll 1$.

By comparing (43) with (47), we conclude that the SSA-1 NRCS for an anisotropic power-law spectrum surface at near-specular direction coincides (apart from the almost-unitary factor a) with the classical GO solution, provided that effective surface slope variances in (44) are used, that change with frequency, via k, and with the incidence and scattering angles, via u_z, see (40).

IV. Validation of the Proposed Approach

In this section, we first verify that the assumptions made to derive (32) and (33) are usually satisfied by natural surfaces, and then, we compare numerical results obtained via (32) and (33) with available measured data and with results of the second-order SSA (SSA-2) [17]. Note that SSA-2 is more accurate than SSA-1, so that it can be used as a reference; however, it requires the numerical computation of fourfold integrals with oscillating integrands, so that it is computationally very heavy, and it requires specific numerical algorithms [17].

A. Validity of the Assumptions

The main assumptions that we have made are as follows.

1) The surface has an anisotropic power-law spectrum in the range of scale lengths actually involved in the scattering process.
2) The surface slope variance, measured at the scale lengths actually involved in the scattering process, is small with respect to unity, so that the validity limits of SSA-1 are satisfied.
3) The anisotropy parameter δ is not larger than about 0.2.
4) $k^2u_z^2s^2l^{2H}\gg 1$.

From [4], [5], [6], and [7], it is known that natural soil surfaces exhibit power-law spectra over range of scales varying from few centimeters to tens of meters (and even at topographic scale, but sometimes with different power exponents α at these larger scales). Typical values of H for soil surfaces are in the range 0.6–0.9, while the order of magnitude of s^2 usually ranges from 10^{-4} to 10^{-2} $\mathrm{m}^{2-2\mathrm{H}}$ [6], [26], [27], [28]. No reliable information on δ or Δ is available for soil surfaces.

With regard to sea surfaces, for microwave scattering purposes, the Elfouhaily spectrum [29] is usually employed. It turns out (e.g., [30] and Fig. 2) that this spectrum is well approximated by (1)–(3) in its high-frequency part, i.e., in the range of surface wavenumbers from several tens of times the peak wavenumber κ_p to about κ_m, where [29]

$$\kappa_p \cong 0.71\frac{g}{u_{10}^2},\ \kappa_m \cong 370\mathrm{m}^{-1},\ g\cong 9.81\mathrm{m/s}^2 \tag{48}$$

and u_{10} is the wind speed at 10 m over the sea surface. For wind speed ranging from 5 to 25 m/s, κ_p ranges from about 0.01 to about 0.25 m^{-1}. In addition, $\alpha=3.5$, so that $H=0.75$, and [30]

$$S_0=\frac{\pi\alpha_m c_m}{\sqrt{g}} \tag{49}$$

where $c_m=0.23$ m/s and α_m is the is the generalized Phillips–Kitaigorodskii equilibrium range parameter, whose expression as an increasing function of wind speed is provided in [29]. Finally, Δ increases with the wind speed according to the expressions reported in [29]. Actually, Δ is also slightly dependent on the surface wavenumber κ, but we can neglect this dependence and take Δ equal to its value at the wavenumber most contributing to the scattering process (κ_B or $2\pi/\rho_0$, according to the value of Ω). For wind speed ranging from 5 to 25 m/s, S_0 [and hence, see (18), s^2] ranges from about 10^{-3} $\mathrm{m}^{2-2\mathrm{H}}$ to about 10^{-2} $\mathrm{m}^{2-2\mathrm{H}}$ and Δ from about 0.2 to about 0.6, so that, see (19), δ ranges from about 0.08 to about 0.25. Note that for higher wind speeds, the scattering is dominated by breaking waves, so that surface scattering models are not accurate at those wind regimes.

From the above data, it is clear that the condition over δ is satisfied for most sea surfaces, the most critical situation being high frequency (Ku-band) at high wind speed. It is reasonable to expect that this condition is satisfied for most soil surfaces, too.

In order to verify the validity of the other assumptions, it is useful to note that the quantity s^2k^{2-2H} is a small fraction of unity for frequencies up to the Ku-band at least. Accordingly, see (31), the parameter Ω is small at far-from-specular directions, where both u_ρ and u_z are of the order of unity and large at near-specular directions, where u_ρ is much smaller than unity. Therefore, to verify that SSA-1 validity limits are satisfied, at far-from-specular directions, the slope variance at the Bragg wavelength scale must be checked, whereas at near-specular direction, the slope variance at the ρ_0 scale must be verified. In the former case, we have (after average over ψ)

$$\sigma_s^2\left(\frac{\Lambda_B}{2\pi}\right)=s^2/\left(\frac{\Lambda_B}{2\pi}\right)^{2-2H}=s^2\kappa_B^{2-2H}=s^2k^{2-2H}u_\rho^{2-2H} \tag{50}$$

which is of the order of no more than s^2k^{2-2H} (since $|u_\rho|$ is smaller than 2), and it is therefore much smaller than unity for natural surfaces, so that SSA-1 can be applied. In addition, for all frequencies spanning from hundreds of MHz to about 12 GHz, the Bragg wavelength is within the range of scales, in which natural surfaces exhibit power-law spectra.

For near-specular directions, we have

$$\sigma_s^2(\rho_0)=s^2/\rho_0^{2-2H}=\frac{\left(\frac{1}{2}k^2s^2u_z^2\right)^{\frac{1}{H}}}{\frac{1}{2}k^2u_z^2}=\left(s^2k^{2-2H}\right)^{\frac{1}{H}}\left(\frac{1}{2}u_z^2\right)^{\frac{1-H}{H}} \tag{51}$$

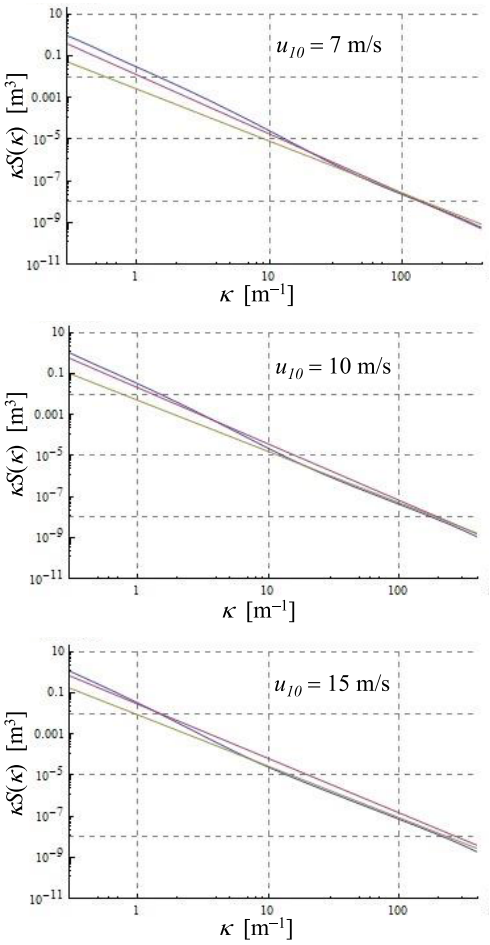

Fig. 2. Elfouhaily spectrum (blue line) and its power-law approximations of (49) (green line) and (52) and (53) (red line) for three different wind velocities.

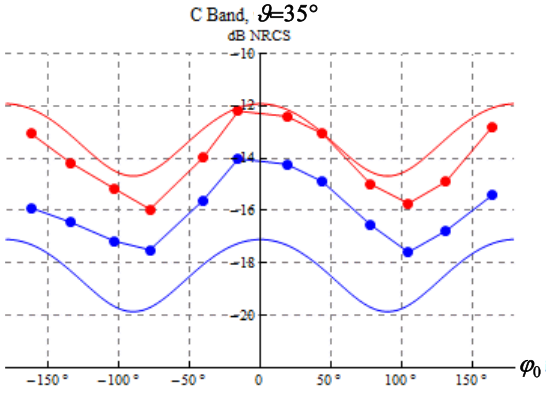

Fig. 3. Backscattering dependence on wind direction ϕ_0 at C-band (frequency = 5.66 GHz and $\varepsilon = 67 - j36$), $\vartheta = 35°$, and $u_{10} = 10$ m/s. Backscattering vv (red line) and hh (blue line) NRCS computed by our method (solid lines) and corresponding measured data (red and blue connected dots).

which is much smaller than unity (since u_z is smaller than 2, too), so that, again, SSA-1 can be applied. In addition, in most cases of interest, the scale lengths of the order of ρ_0 turn out to be within the range of scales, in which natural surfaces exhibit power-law spectra. A noteworthy exception is the sea surface when L-band is used: in this case, in fact, at low (up to about 10 m/s) wind speed, $2\pi/\rho_0$ is of the order of no more than few tens of times κ_p, so that the power-law model with $\alpha = 3.5$ and S_0 given by (49) is not a good approximation of the Elfouhaily spectrum. However, as shown in [31] and as illustrated in Fig. 2, in this more extended range of wavenumbers, a still reasonably good agreement with the Elfouhaily spectrum is obtained by using a wind-dependent parameter α given by

$$\alpha = 3.5 + 0.5 \exp\left(-\frac{u_{10}^2}{u_0^2}\right) \tag{52}$$

where $u_0 = 12$ m/s, and replacing (49) with

$$S_0 = C\alpha_m \left[1 + \exp\left(-\frac{u_{10}^2}{u_0^2}\right)\right] \tag{53}$$

where $C = 0.623$ m$^{4-\alpha}$.

Finally, we note that, considering the range of values of s^2 and H of natural surfaces, the condition $k^2 u_z^2 s^2 l^{2H} \gg 1$ is satisfied if the linear size l of the illuminated surface patch is much larger than wavelength.

B. Numerical Results

Let us first consider a comparison of our NRCS results with real backscattering measurements over the sea available in literature.

In Fig. 3, we illustrate the dependence on wind direction ϕ_0 of vv and hh backscattering NRCSs ($\vartheta_s = \vartheta_i$ and $\varphi_s = \pi$) for a wind speed $u_{10} = 10$ m/s, at C-band (frequency = 5.66 GHz and $\varepsilon = 67 - j36$) and $\vartheta_i = 35°$. Measurements obtained from RADARSAT-2 quad-pol synthetic aperture radar (SAR) data, reported in [32], are also shown in Fig. 3. Similarly, in Fig. 4, we show the vv and hh backscattering NRCSs as functions of wind direction ϕ_0 for a wind speed $u_{10} = 10$ m/s, at Ku-band (frequency = 12.5 GHz and $\varepsilon = 42 - j39$) and $\vartheta_i = 45°$. Measurements obtained by using an aircraft polarimetric scatterometer, reported in [33], are also displayed in Fig. 4. In both cases, a good agreement with measurements is obtained at vv polarization, whereas an underestimation of about 3 dB is obtained at hh polarization. However, a similar underestimation with respect to backscattering measurements at hh polarization is also obtained by using the more refined SSA-2, see for instance [17]. This discrepancy is mainly due to the presence of breaking waves [17], [34], [35], which causes an asymmetry in the wave shape and the presence of foam: both phenomena are not considered in the employed sea surface description, and their effects are much more pronounced at hh polarization than at vv polarization [17], [34]. The discrepancy can be strongly reduced by using, for instance, the empirical correction functions provided in [34]. However, this is beyond the scope of our work.

Let us now move to consider comparisons with SSA-2 results. In Fig. 5, we show vv and hh backscattering NRCS as a function of the incidence angle ϑ_i at X-band (frequency = 10 GHz and $\varepsilon = 61 - j45$) for a wind speed $u_{10} = 15$ m/s, and for up-wind ($\phi_0 = 0$) and obliquus wind direction ($\phi_0 = 45°$). This case is the same as considered in [17, Fig. 3], so that we can directly compare our results with those obtained in [17] by using SSA-2. It turns out that a

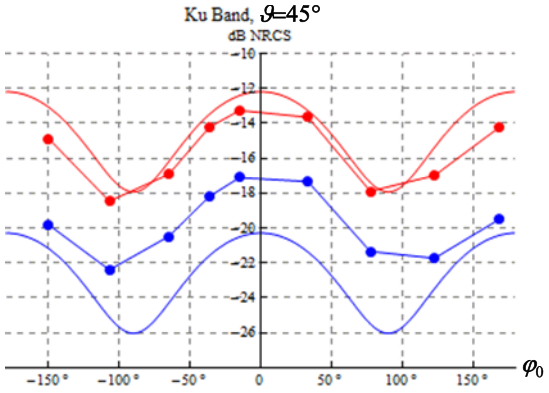

Fig. 4. Backscattering dependence on wind direction ϕ_0 at Ku-band (frequency = 12.5 GHz and $\varepsilon = 42 - j39$), $\vartheta = 45°$, and $u_{10} = 10$ m/s. Backscattering vv (red line) and hh (blue line) NRCS computed by our method (solid lines) and corresponding measured data (red and blue connected dots).

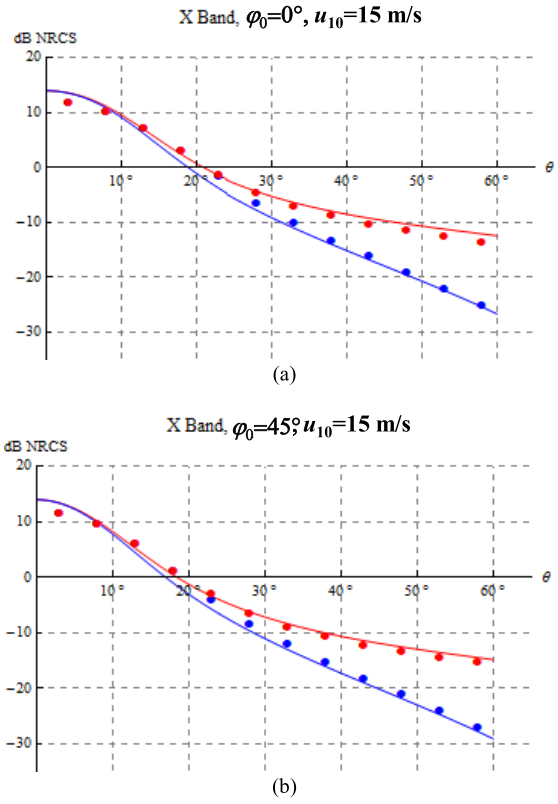

Fig. 5. Backscattering NRCS at vv (red line) and hh (blue line) polarizations versus the incidence angle ϑ at X-band (frequency = 10 GHz and $\varepsilon = 61 - j45$) for $u_{10} = 15$ m/s and for (a) up-wind ($\phi_0 = 0$) and (b) obliquus wind direction ($\phi_0 = 45°$). Our model (solid lines) is compared with SSA-2 (dots).

satisfactory agreement is obtained, also considering that results of [17] are obtained not only with a higher order model, but also using the exact Elfouhaily spectrum, at variance with our power-law approximation [we used $\alpha = 3.5$ and S_0 given by (49), which is appropriate at C-, X-, and Ku-bands at nonnegligible wind speed, see Section IV-A].

Let us now consider a bistatic scattering case. In Fig. 6, we illustrate the sea surface bistatic NRCSs, as a function of the polar scattering angle ϑ_s, for up-wind ($\phi_0 = 0$) configuration and for several azimuth scattering angles φ_s, with an incidence angle $\vartheta_i = 45°$, at L-band (frequency = 1.58 GHz

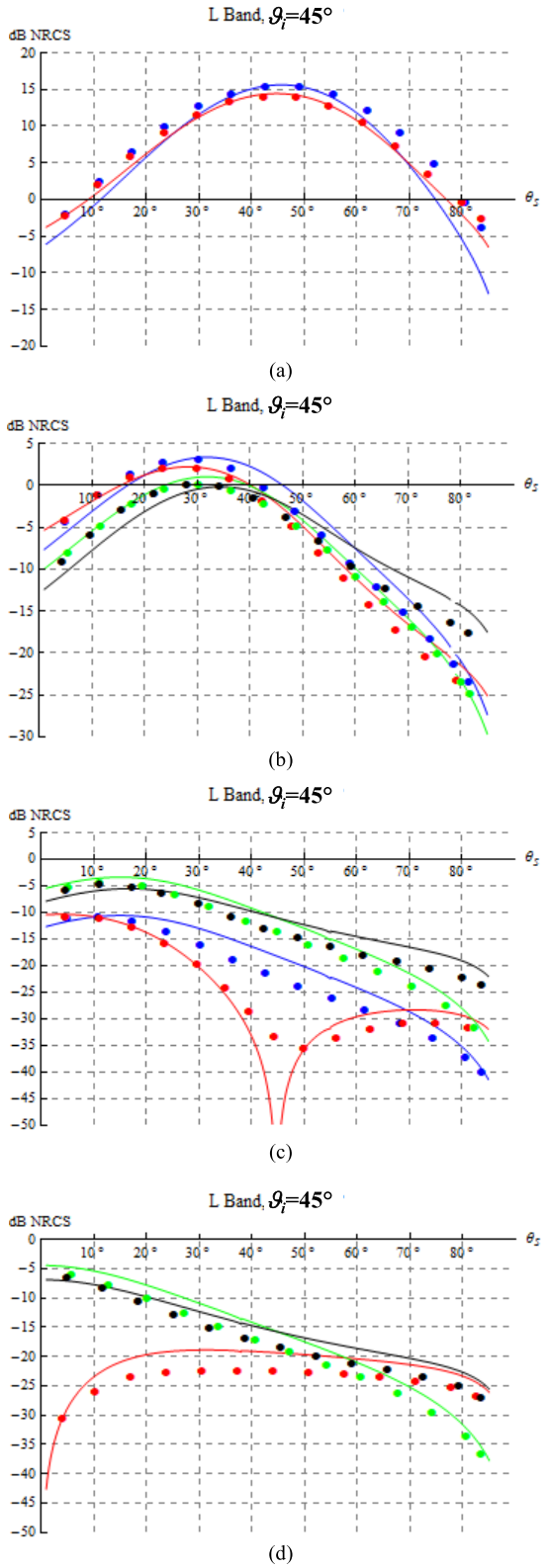

Fig. 6. Bistatic NRCS (hh in blue, vv in red, hv in green, and vh in black) versus the polar scattering angle ϑ_s at L-band (frequency = 1.58 GHz and $\varepsilon = 65 - j61$) for $\vartheta_i = 45°$, a sea surface with $u_{10} = 10$ m/s, up-wind ($\phi_0 = 0$), and azimuth scattering angles: (a) $\phi_s = 0°$, (b) $\phi_s = 30°$, (c) $\phi_s = 60°$, and (d) $\phi_s = 90°$. The results obtained with the SSA-2 model are reported as dots (hh in blue, vv in red, hv in green, and vh in black).

and $\varepsilon = 65 - j61$), and for a wind speed $u_{10} = 10$ m/s. Again, this specific configuration is the same considered in [17], and

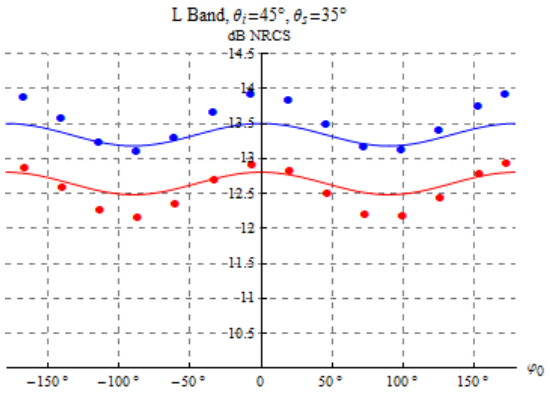

Fig. 7. Bistatic NRCS (*hh* in blue and *vv* in red) versus wind direction ϕ_0 at L-band (frequency = 1.58 GHz and $\varepsilon = 65 - j61$) for $\vartheta_i = 45°$, for a sea surface with $u_{10} = 10$ m/s, $\phi_s = 0°$, and $\vartheta_s = 35°$. The results obtained with the SSA-2 model are reported as dots (*hh* in blue and *vv* in red).

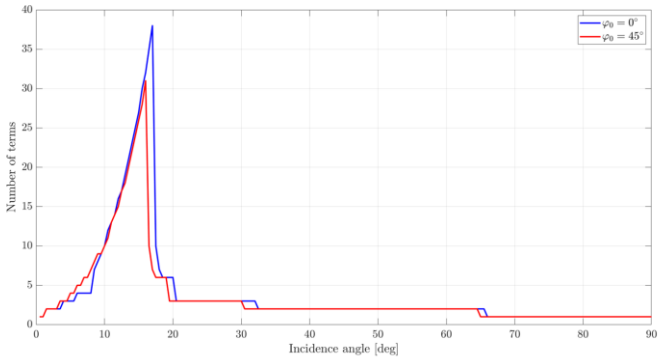

Fig. 8. Number of terms needed to compute the NRCS of Fig. 5, as a function of the incidence angle. In this plot, the number of terms is $n = \min\{n_1, n_2\}$, where n_1 and n_2 are the numbers of terms needed to converge by the series (32) and (33), respectively.

results obtained there via SSA-2 (and considering the exact Elfouhaily spectrum) are also shown in Fig. 6. In this case, in our method, we used α and S_0 given by (52) and (53), which is appropriate at L-band (see Section IV-A). A good agreement is obtained in almost all cases, with differences of no more than about 3 dB, except, in a few cases, at grazing scattering angles. In addition, a very low *vv* polarization NRCS is obtained by our method at $\vartheta_s \cong 45°$ for $\varphi_s = 60°$ [see Fig. 6(c)] and at $\vartheta_s \cong 0°$ for $\varphi_s = 90°$ [see Fig. 6(d)]. This is an intrinsic limitation of SSA-1: in fact, if, as it is the case for the sea surface, $|\varepsilon| \gg 1$, the Bragg coefficient B_{vv}, see (25), becomes negligible when $\cos\varphi_s = \sin\vartheta_s \sin\vartheta_i$.

Finally, in Fig. 7, we show the sea surface NRCS behavior as a function of wind direction ϕ_0 at L-band (frequency = 1.58 GHz and $\varepsilon = 65 - j61$) for $u_{10} = 10$ m/s, $\vartheta_i = 45°$, $\vartheta_s = 35°$, and $\phi_s = 0°$. Again, our results are compared to those obtained via SSA-2 in [17], and a reasonable agreement is obtained.

A few last words on computational complexity are now needed. It turns out that in most cases of practical interest, at least one of the two series, (32) and (33), converges after very few terms. Here, for "converges," we mean that the absolute value of the difference in decibel (dB) between the values obtained by arresting the summation after $n + 1$ and

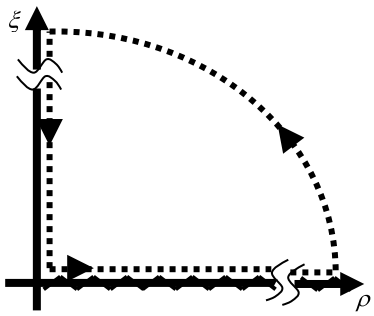

Fig. 9. Integration contour for the integrals in (30) in the complex $p = \rho + j\xi$ plane.

n terms falls below a prescribed threshold. For instance, in Fig. 8, we plot the number of terms, as a function of the incidence angle, needed to compute the NRCS in the case of Fig. 5 with an accuracy of 0.1 dB. In particular, the expression (33) is used for small incidence angles, up to 16°–17°, whereas (32) is used for larger incidence angles. The number of needed terms is always smaller than five, except for incidence angles around 16°–17°, where Ω is of the order of unity and the number of terms is up to more than 30. In any case, all the plots in Figs. 3–7 have been obtained in less than 1 s by using a commonly available laptop.

V. Conclusion

In this article, we have presented an analytical method to compute the NRCS of anisotropic power-law spectrum surfaces. The method extends to the anisotropic case the approach of [7], [11], [12], [13], [14], and [18]. In particular, first of all, we have evaluated the structure function of an anisotropic 2-D random process with power-law PSD, and we have thus shown that this process can be considered as the anisotropic generalization of an fBm process. Then, we have used this process to model natural surfaces, and we have derived an analytical formulation of their NRCS by using the SSA-1. We have also verified that at far-from-specular scattering, our formulation tends to the SPM one, whereas at near-specular scattering, it tends to the GO expression with properly defined effective surface slope variances. Finally, we have compared the obtained results with measured NRCSs of natural surfaces and with NRCS values obtained via the SSA-2. The presented results suggest that our approach can be used for a reasonably accurate fast evaluation of NRCS of natural surfaces. It must be underlined that, at variance with the TSM, the proposed approach does not require the (to some extent arbitrary) definition of a cutoff surface wavenumber. Our approach inherits this advantage from the SSA-1. However, without using our approach, the application of the SSA-1 to scattering from surfaces described by a power-law-like spectrum (for instance, the Elfouhaily spectrum [29], [35]) requires a numerical integration for the inverse Fourier transform of the surface spectrum to derive the surface correlation function (or structure function) and then a numerical integration to evaluate the scattering integral in (23). Conversely, we perform both integrations analytically, so that no numerical integration is needed, and a fully analytical

formulation is obtained. This greatly reduces computational time and allows a deeper physical insight (see, for instance, the discussion in Section III-B).

It must finally be noted that the presented approach also inherits the limitations of the SSA-1 that, as all the first-order scattering models, does not account for multiple scattering and is not able to model cross-polarization in backscattering and, more in general, depolarization effects of rough surface scattering. In the cases in which these effects need to be accounted for, a fast evaluation of scattering can be obtained with the anisotropic polarimetric two-scale model (A-PTSM) method of [10] and [30], which is a TSM approach, in which the effect of the choice of the cutoff wavenumber on the final NRCS is reduced by using a semiempirical method to evaluate surface slope variances.

Appendix A

In this Appendix, we show how (11) is obtained.

By making the substitution $\vartheta = \varphi - \psi$, exploiting the periodicity of the integrand, and finally considering that cosine and sine are even and odd functions, respectively, we have

$$\begin{aligned}
&\int_0^{2\pi} e^{j\bar{\kappa}\cos(\varphi-\psi)}\cos[2(\varphi-\varphi_0)]d\varphi \\
&\quad= \int_{-\psi}^{2\pi-\psi} e^{j\bar{\kappa}\cos\vartheta}\cos[2\vartheta+2(\psi-\varphi_0)]d\vartheta \\
&\quad= \int_{-\pi}^{+\pi} e^{j\bar{\kappa}\cos\vartheta}\{\cos 2\vartheta\cos[2(\psi-\varphi_0)] \\
&\qquad- \sin 2\vartheta\sin[2(\psi-\varphi_0)]\}d\vartheta \\
&\quad= 2\cos[2(\psi-\varphi_0)]\int_0^{\pi} e^{j\bar{\kappa}\cos\vartheta}\cos 2\vartheta\, d\vartheta. \qquad (54)
\end{aligned}$$

By using the following expression of the νth-order Bessel function of the first kind [20]

$$J_\nu(\bar{\kappa}) = \frac{j^{-\nu}}{\pi}\int_0^{\pi} e^{j\bar{\kappa}\cos\vartheta}\cos(\nu\vartheta)d\vartheta \qquad (55)$$

with $\nu = 2$, in (54), we obtain (11).

Appendix B

In this Appendix, we evaluate the following integrals, appearing in (30), under the hypothesis that the parameter Ω defined in (31) is small:

$$\begin{aligned}
&\int_0^{\infty} J_0(ku_\rho\rho)e^{-\frac{1}{2}k^2u_z^2s^2\rho^{2H}}\rho d\rho \\
&\quad= \mathrm{Re}\left\{\int_0^{\infty} H_0(ku_\rho\rho)e^{-\frac{1}{2}k^2u_z^2s^2\rho^{2H}}\rho d\rho\right\} \qquad (56) \\
&\int_0^{\infty} J_2(ku_\rho\rho)e^{-\frac{1}{2}k^2u_z^2s^2\rho^{2H}}\rho^{1+2H}d\rho \\
&\quad= \mathrm{Re}\left\{\int_0^{\infty} H_2(ku_\rho\rho)e^{-\frac{1}{2}k^2u_z^2s^2\rho^{2H}}\rho^{1+2H}d\rho\right\} \qquad (57)
\end{aligned}$$

where $H_\nu(\cdot)$ is the νth-order Hankel function of the first kind [20], and $\mathrm{Re}\{H_\nu(\cdot)\} = J_\nu(\cdot)$. We take the analytical continuation of the integrands of (56) and (57) on the complex plane $p = \rho + j\xi$, and we consider a cut along the real positive axis in order to force the function p^{2H} to be single-valued.

Integration along the contour depicted in Fig. 9 leads to

$$\begin{aligned}
&\mathrm{Re}\left\{\oint H_\nu(ku_\rho p)e^{-\frac{1}{2}k^2u_z^2s^2p^{2H}}p^{1+\nu H}dp\right\} \\
&= \int_0^{\infty} J_\nu(ku_\rho\rho)e^{-\frac{1}{2}k^2u_z^2s^2\rho^{2H}}\rho^{1+\nu H}d\rho \\
&\quad- \mathrm{Re}\left\{\int_0^{j\infty} H_\nu(ku_\rho j\xi)e^{-\frac{1}{2}k^2u_z^2s^2(j\xi)^{2H}}(j\xi)^{1+\nu H}d(j\xi)\right\} \\
&= 0 \qquad (58)
\end{aligned}$$

where $\nu = 0$ for the case of (56) and $\nu = 2$ for the case of (57).

From (58), we get

$$\begin{aligned}
&\int_0^{\infty} J_\nu(ku_\rho\rho)e^{-\frac{1}{2}k^2u_z^2s^2\rho^{2H}}\rho^{1+\nu H}d\rho \\
&\quad= \mathrm{Re}\left\{\frac{2}{\pi}(-1)^{1+\frac{\nu}{2}}j^{\nu H-1}\int_0^{\infty} K_\nu(ku_\rho\xi)\right. \\
&\qquad\left.\times e^{-\frac{1}{2}k^2u_z^2s^2(j\xi)^{2H}}\xi^{1+\nu H}d\xi\right\} \qquad (59)
\end{aligned}$$

where $K_\nu(t) = (\pi j^{1+\nu}/2)H_\nu(jt)$ is the νth-order modified Bessel function of the second kind [20]. This function has an exponential decay, so that $\mathrm{K}_\nu(ku_\rho\xi)$ is appreciably different from zero only for values of ξ smaller than a few times $1/(ku_\rho)$. If Ω is small, for such values of ξ, the argument of the exponential in (59) is small, so that it is convenient to expand this exponential in Taylor series around null argument

$$e^{-\frac{1}{2}k^2u_z^2s^2(j\xi)^{2H}} = \sum_{n=0}^{\infty}\frac{(-1)^n}{n!}\left(\frac{1}{2}k^2u_z^2s^2\right)^n j^{2nH}\xi^{2nH}. \qquad (60)$$

It can also be noted that the main contribution to the integral in (59) comes from the values of ξ around $1/ku_\rho = \Lambda_B/2\pi$, so that the scale lengths involved in the scattering phenomenon are those around the Bragg wavelength.

Substitution of (60) in (59) and integration by series lead to

$$\begin{aligned}
&\int_0^{\infty} J_\nu(ku_\rho\rho)e^{-\frac{1}{2}k^2u_z^2s^2\rho^{2H}}\rho^{1+\nu H}d\rho \\
&\quad= \frac{2}{\pi}\sum_{n=0}^{\infty}\mathrm{Re}\left\{j^{(n+\frac{\nu}{2})2H-1}\right\}\frac{(-1)^{n+1+\frac{\nu}{2}}}{n!}\left(\frac{1}{2}k^2u_z^2s^2\right)^n \\
&\qquad\cdot\int_0^{\infty} K_\nu(ku_\rho\xi)\xi^{(n+\frac{\nu}{2})2H+1}d\xi. \qquad (61)
\end{aligned}$$

By noting that

$$\begin{aligned}
&\mathrm{Re}\left\{j^{(n+\frac{\nu}{2})2H-1}\right\} \\
&\quad= \cos\left[\left(n+\frac{\nu}{2}\right)\pi H-\frac{\pi}{2}\right] = \sin\left[\left(n+\frac{\nu}{2}\right)\pi H\right]
\end{aligned}$$

and using the following equality [21]:

$$\int_0^{\infty} K_\nu(u\xi)\xi^\mu d\xi = 2^{\mu-1}u^{-\mu-1}\Gamma\left(\frac{1+\mu-\nu}{2}\right)\Gamma\left(\frac{1+\mu+\nu}{2}\right) \qquad (62)$$

that holds for $\mu \pm \nu > -1$, with $\mu = (n+\nu/2)2H+1$, $\nu = 0, 2$ and $u = ku_\rho$, we get

$$\begin{aligned}\int_0^\infty & J_\nu(ku_\rho\rho)\mathrm{e}^{-\frac{1}{2}k^2u_z^2s^2\rho^{2H}}\rho^{1+\nu H}d\rho \\ &= \frac{2}{\pi}\sum_{n=0}^{\infty}\frac{(-1)^{n+1+\frac{\nu}{2}}2^{(n+\frac{\nu}{2})2H}\sin\left[\left(n+\frac{\nu}{2}\right)\pi H\right]}{n!} \\ &\quad\times\Gamma\left[\left(n+\frac{\nu}{2}\right)H+1-\frac{\nu}{2}\right]\Gamma\left[\left(n+\frac{\nu}{2}\right)H+1+\frac{\nu}{2}\right] \\ &\quad\times\frac{\left(\frac{1}{2}k^2u_z^2s^2\right)^n}{\left(k^2u_\rho^2\right)^{(n+\frac{\nu}{2})H+1}} \\ &= \frac{2}{\pi}\sum_{n=\nu/2}^{\infty}\frac{(-1)^{n+1}2^{2nH}\sin[n\pi H]}{\left(n-\frac{\nu}{2}\right)!}\Gamma\left[1+nH-\frac{\nu}{2}\right] \\ &\quad\times\Gamma\left[1+nH+\frac{\nu}{2}\right]\frac{\left(\frac{1}{2}k^2u_z^2s^2\right)^{n-\frac{\nu}{2}}}{\left(k^2u_\rho^2\right)^{nH+1}}. \end{aligned} \tag{63}$$

Use of the relation [20]

$$\sin[n\pi H] = \frac{n\pi H}{\Gamma[1+nH]\Gamma[1-nH]} \tag{64}$$

in (63) leads to

$$\begin{aligned}\int_0^\infty & \mathrm{J}_\nu(ku_\rho\rho)\mathrm{e}^{-\frac{1}{2}k^2u_z^2s^2\rho^{2H}}\rho^{1+\nu H}d\rho \\ &= 2H\sum_{n=1}^{\infty}\frac{(-1)^{n+1}2^{2nH}}{\left(n-\frac{\nu}{2}\right)!}\frac{n\Gamma\left[1+nH-\frac{\nu}{2}\right]\Gamma\left[1+nH+\frac{\nu}{2}\right]}{\Gamma[1+nH]\Gamma[1-nH]} \\ &\quad\times\frac{\left(\frac{1}{2}k^2u_z^2s^2\right)^{n-\frac{\nu}{2}}}{\left(k^2u_\rho^2\right)^{nH+1}}. \end{aligned} \tag{65}$$

For $\nu = 0$, we obtain

$$\begin{aligned}\int_0^\infty & J_0(ku_\rho\rho)\mathrm{e}^{-\frac{1}{2}k^2u_z^2s^2\rho^{2H}}\rho d\rho \\ &= 2H\sum_{n=1}^{\infty}\frac{(-1)^{n+1}2^{2nH}}{n!}\frac{n\Gamma[1+nH]}{\Gamma[1-nH]}\frac{\left(\frac{1}{2}k^2u_z^2s^2\right)^n}{\left(k^2u_\rho^2\right)^{nH+1}} \end{aligned} \tag{66}$$

while for $\nu = 2$, we get

$$\begin{aligned}\int_0^\infty & J_2(ku_\rho\rho)\mathrm{e}^{-\frac{1}{2}k^2u_z^2s^2\rho^{2H}}\rho^{1+2H}d\rho \\ &= 2H\sum_{n=1}^{\infty}\frac{(-1)^{n+1}2^{2nH}}{(n-1)!}\frac{n\Gamma[nH]\Gamma[2+nH]}{\Gamma[1+nH]\Gamma[1-nH]}\frac{\left(\frac{1}{2}k^2u_z^2s^2\right)^{n-1}}{\left(k^2u_\rho^2\right)^{nH+1}} \\ &= 2H\sum_{n=1}^{\infty}\frac{(-1)^{n+1}2^{2nH}}{n!}\frac{n(1+nH)\Gamma[1+nH]}{H\Gamma[1-nH]}\frac{\left(\frac{1}{2}k^2u_z^2s^2\right)^{n-1}}{\left(k^2u_\rho^2\right)^{nH+1}} \end{aligned} \tag{67}$$

where we have used $1/(n-1)! = n/n!$ and [20]

$$\Gamma(1+t) = t\Gamma(t) \tag{68}$$

so that

$$\frac{\Gamma(nH)}{\Gamma(1+nH)} = \frac{1}{nH}, \Gamma(2+nH) = (1+nH)\Gamma(1+nH). \tag{69}$$

By employing (66) and (67) in (30), we readily obtain (32).

A rigorous proof that the series in (66) and (67) are asymptotic expansions of the corresponding integrals for $\Omega \to 0$ can be obtained by proceeding along a line similar to the one described in [25] for the isotropic case.

APPENDIX C

In this Appendix, we consider the case of large values of the parameter Ω defined in (31). First of all, we note that the second exponential in (27) is appreciably different from zero only for values of ρ smaller than a few times ρ_0 defined in (39). If Ω is large, for such values of ρ, the argument of the first exponential in (27) is small, and this first exponential is approximately unitary. Therefore, the main contribution to the integral in (27) comes from the values of ρ around ρ_0, so that the scale lengths involved in the scattering phenomenon are those around ρ_0.

Let us now consider the integrals

$$\int_0^\infty J_\nu(ku_\rho\rho)\mathrm{e}^{-\frac{1}{2}k^2u_z^2s^2\rho^{2H}}\rho^{1+\nu H}d\rho \tag{70}$$

with $\nu = 0$ and $\nu = 2$ that appear in (30). The exponential appearing in (70) is appreciably different from zero only for values of ρ smaller than a few times $1/((1/2)k^2s^2u_z^2)^{1/2H}$. If Ω is large, for such values of ρ, the argument of the Bessel function in (70) is small, so that it is convenient to expand the Bessel function in Taylor series around null argument [20]

$$J_\nu(ku_\rho\rho) = \sum_{n=0}^{\infty}\frac{(-1)^n}{n!(n+\nu)!}\left(\frac{1}{2}ku_\rho\rho\right)^{2n+\nu}. \tag{71}$$

Substitution of (71) in (70) and integration by series lead to

$$\begin{aligned}\int_0^\infty & J_\nu(ku_\rho\rho)\mathrm{e}^{-\frac{1}{2}k^2u_z^2s^2\rho^{2H}}\rho^{1+\nu H}d\rho \\ &= \sum_{n=0}^{\infty}\frac{(-1)^n\left(k^2u_\rho^2\right)^{n+\frac{\nu}{2}}}{2^{2n+\nu}n!(n+\nu)!}\int_0^\infty \mathrm{e}^{-\frac{1}{2}k^2u_z^2s^2\rho^{2H}}\rho^{2\left(n+\frac{\nu}{2}\right)+1+\nu H}d\rho. \end{aligned} \tag{72}$$

By using the following equality [21]:

$$\int_0^\infty \mathrm{e}^{-u\rho^{2H}}\rho^w d\rho = \frac{1}{2H}\frac{1}{u^{\frac{w+1}{2H}}}\Gamma\left(\frac{w+1}{2H}\right) \tag{73}$$

that holds for $w > -1$, with $w = 2(n+\nu/2)+1+\nu H$ and $u = (1/2)k^2u_z^2s^2$, we get

$$\begin{aligned}\int_0^\infty & J_\nu(ku_\rho\rho)\mathrm{e}^{-\frac{1}{2}k^2u_z^2s^2\rho^{2H}}\rho^{1+\nu H}d\rho \\ &= \frac{1}{2H}\sum_{n=0}^{\infty}\frac{(-1)^n}{2^{2n+\nu}n!(n+\nu)!}\Gamma\left(\frac{\left(n+\frac{\nu}{2}\right)+1}{H}+\frac{\nu}{2}\right) \\ &\quad\times\frac{\left(k^2u_\rho^2\right)^{n+\frac{\nu}{2}}}{\left(\frac{1}{2}k^2u_z^2s^2\right)^{\frac{\left(n+\frac{\nu}{2}\right)+1}{H}+\frac{\nu}{2}}} \\ &= \frac{1}{2H}\sum_{n=\nu/2}^{\infty}\frac{(-1)^{n-\frac{\nu}{2}}}{2^{2n}\left(n-\frac{\nu}{2}\right)!\left(n+\frac{\nu}{2}\right)!}\Gamma\left(\frac{n+1}{H}+\frac{\nu}{2}\right) \\ &\quad\times\frac{\left(k^2u_\rho^2\right)^n}{\left(\frac{1}{2}k^2u_z^2s^2\right)^{\frac{n+1}{H}+\frac{\nu}{2}}}. \end{aligned} \tag{74}$$

For $\nu = 0$, we obtain

$$\int_0^\infty J_0\left(ku_\rho\rho\right)\mathrm{e}^{-\frac{1}{2}k^2u_z^2s^2\rho^{2H}}\rho d\rho = \frac{1}{2H}\sum_{n=0}^{\infty}\frac{(-1)^n}{2^{2n}(n!)^2}\Gamma\left(\frac{n+1}{H}\right)\frac{\left(k^2u_\rho^2\right)^n}{\left(\frac{1}{2}k^2u_z^2s^2\right)^{\frac{n+1}{H}}} \tag{75}$$

while for $\nu = 2$, we get

$$\begin{aligned}\int_0^\infty J_2\left(ku_\rho\rho\right)\mathrm{e}^{-\frac{1}{2}k^2u_z^2s^2\rho^{2H}}\rho^{1+2H}d\rho &= \frac{1}{2H}\sum_{n=1}^{\infty}\frac{(-1)^{n-1}}{2^{2n}(n-1)!(n+1)!}\Gamma\left(\frac{n+1}{H}+1\right)\frac{\left(k^2u_\rho^2\right)^n}{\left(\frac{1}{2}k^2u_z^2s^2\right)^{\frac{n+1}{H}+1}}\\ &= \frac{1}{2H}\sum_{n=1}^{\infty}\frac{(-1)^{n-1}}{2^{2n}(n!)^2}\frac{n}{H}\Gamma\left(\frac{n+1}{H}\right)\frac{\left(k^2u_\rho^2\right)^n}{\left(\frac{1}{2}k^2u_z^2s^2\right)^{\frac{n+1}{H}+1}}\end{aligned} \tag{76}$$

where we have used (68), so that

$$\Gamma\left(\frac{n+1}{H}+1\right) = \frac{n+1}{H}\Gamma\left(\frac{n+1}{H}\right),\ \frac{1}{(n-1)!} = \frac{n}{n!}$$

and

$$\frac{n+1}{(n+1)!} = \frac{1}{n!}.$$

By employing (75) and (76) in (30), we readily obtain (33).

A rigorous proof that the series in (75) and (76) are asymptotic expansions of the corresponding integrals for $\Omega \to \infty$ can be obtained by proceeding along a line similar to the one described in [25] for the isotropic case.

REFERENCES

[1] F. T. Ulaby, R. K. Moore, and A. K. Fung, *Microwave Remote Sensing: Active and Passive*. Reading, MA, USA: Addison-Wesley, 1982.

[2] L. Tsang, J. A. Kong, and R. T. Shin, *Theory of Microwave Remote Sensing*. New York, NY, USA: Wiley, 1985.

[3] A. K. Fung, *Microwave Scattering and Emission: Models and Their Applications*. Norwood, MA, USA: Artech House, 1994.

[4] B. B. Mandelbrot, *The Fractal Geometry of Nature*. New York, NY, USA: W. H. Freeman, 1983.

[5] K. Falconer, *Fractal Geometry*. New York, NY, USA: Wiley, 1990.

[6] B. A. Campbell, "Scale-dependent surface roughness behavior and its impact on empirical models for radar backscatter," *IEEE Trans. Geosci. Remote Sens.*, vol. 47, no. 10, pp. 3480–3488, Oct. 2009.

[7] G. Franceschetti, A. Iodice, M. Migliaccio, and D. Riccio, "Scattering from natural rough surfaces modeled by fractional Brownian motion two-dimensional processes," *IEEE Trans. Antennas Propag.*, vol. 47, no. 9, pp. 1405–1415, Sep. 1999.

[8] J. Wright, "A new model for sea clutter," *IEEE Trans. Antennas Propag.*, vol. AP-16, no. 2, pp. 217–223, Mar. 1968.

[9] G. R. Valenzuela, "Scattering of electromagnetic waves from a tilted slightly rough surface," *Radio Sci.*, vol. 3, no. 11, pp. 1057–1066, Nov. 1968.

[10] G. Di Martino, A. Di Simone, A. Iodice, and D. Riccio, "Bistatic scattering from anisotropic rough surfaces via a closed-form two-scale model," *IEEE Trans. Geosci. Remote Sens.*, vol. 59, no. 5, pp. 3656–3671, May 2021.

[11] O. I. Yordanov and K. Ivanova, "Kirchhoff diffractals," *J. Phys. A, Math. Gen.*, vol. 27, no. 17, pp. 5979–5993, Sep. 1994.

[12] G. Franceschetti, A. Iodice, and D. Riccio, "Fractal models for scattering from natural surfaces," in *Scattering*, R. Pike and P. Sabatier, Eds. London, U.K.: Academic, 2001, pp. 467–485.

[13] S. Perna and A. Iodice, "On the use of series expansions for Kirchhoff diffractals," *IEEE Trans. Antennas Propag.*, vol. 59, no. 2, pp. 595–610, Feb. 2011.

[14] A. Iodice, A. Natale, and D. Riccio, "Kirchhoff scattering from fractal and classical rough surfaces: Physical interpretation," *IEEE Trans. Antennas Propag.*, vol. 61, no. 4, pp. 2156–2163, Apr. 2013.

[15] K. F. Warnick, F. W. Millet, and D. V. Arnold, "Physical and geometrical optics for 2-D rough surfaces with power-law height spectra," *IEEE Trans. Antennas Propag.*, vol. 53, no. 3, pp. 922–932, Mar. 2005.

[16] A. Voronovich, "Small-slope approximation for electromagnetic wave scattering at a rough interface of two dielectric half-spaces," *Waves Random Media*, vol. 4, no. 3, pp. 337–367, Jul. 1994.

[17] A. G. Voronovich and V. U. Zavorotny, "Full-polarization modeling of monostatic and bistatic radar scattering from a rough sea surface," *IEEE Trans. Antennas Propag.*, vol. 62, no. 3, pp. 1362–1371, Mar. 2014.

[18] A. Iodice, G. Di Martino, A. Di Simone, D. Riccio, and G. Ruello, "Electromagnetic scattering from fractional Brownian motion surfaces via the small slope approximation," *Fractal Fractional*, vol. 7, no. 5, p. 387, May 2023.

[19] A. Ishimaru, *Wave Propagation and Scattering in Random Media*. New York, NY, USA: Academic, 1993.

[20] M. Abramowitz and I. A. Stegun, *Handbook of Mathematical Functions*. New York, NY, USA: Dover, 1970.

[21] I. S. Gradshteyn and I. M. Ryzhik, *Tables of Integrals, Series, and Products*. Orlando, FL, USA: Academic, 1980.

[22] I. S. Reed, P. C. Lee, and T. K. Truong, "Spectral representation of fractional Brownian motion in n dimensions and its properties," *IEEE Trans. Inf. Theory*, vol. 41, no. 5, pp. 1439–1451, Sep. 1995.

[23] W. Fuscaldo, A. Di Simone, L. M. Millefiori, A. Iodice, P. Braca, and P. K. Willett, "A convenient analytical framework for electromagnetic scattering from composite targets," *Radio Sci.*, vol. 54, no. 8, pp. 785–807, Aug. 2019.

[24] A. Di Simone et al., "Analytical models for the electromagnetic scattering from isolated targets in bistatic configuration: Geometrical optics solution," *IEEE Trans. Geosci. Remote Sens.*, vol. 58, no. 2, pp. 861–880, Feb. 2020.

[25] S. Perna and A. Iodice, "Asymptotic behavior of two series used for the evaluation of Kirchhoff diffractals," *IEEE Trans. Antennas Propag.*, vol. 59, no. 6, pp. 2442–2444, Jun. 2011.

[26] S. R. Brown and C. H. Scholz, "Broad bandwidth study of the topography of natural rock surfaces," *J. Geophys. Res., Solid Earth*, vol. 90, no. B14, pp. 12575–12582, Dec. 1985.

[27] R. T. Austin, A. W. England, and G. H. Wakefield, "Special problems in the estimation of power-law spectra as applied to topographical modeling," *IEEE Trans. Geosci. Remote Sens.*, vol. 32, no. 4, pp. 928–939, Jul. 1994.

[28] G. Di Martino, A. Iodice, D. Riccio, and G. Ruello, "Equivalent number of scatterers for SAR speckle modeling," *IEEE Trans. Geosci. Remote Sens.*, vol. 52, no. 5, pp. 2555–2564, May 2014.

[29] T. Elfouhaily, B. Chapron, K. Katsaros, and D. Vandemark, "A unified directional spectrum for long and short wind-driven waves," *J. Geophys. Res., Oceans*, vol. 102, no. C7, pp. 15781–15796, Jul. 1997.

[30] G. Di Martino, A. Iodice, and D. Riccio, "Closed-form anisotropic polarimetric two-scale model for fast evaluation of sea surface backscattering," *IEEE Trans. Geosci. Remote Sens.*, vol. 57, no. 8, pp. 6182–6194, Aug. 2019.

[31] G. Di Martino, A. Di Simone, A. Iodice, D. Riccio, and G. Ruello, "Scattering along the specular direction from the sea modeled as a fractal surface," in *Proc. IEEE Int. Geosci. Remote Sens. Symp. (IGARSS)*, Sep. 2023, pp. 635–637.

[32] B. Zhang et al., "Ocean vector winds retrieval from C-band fully polarimetric SAR measurements," *IEEE Trans. Geosci. Remote Sens.*, vol. 50, no. 11, pp. 4252–4261, Nov. 2012.

[33] S. H. Yueh, W. J. Wilson, and S. Dinardo, "Polarimetric radar remote sensing of ocean surface wind," *IEEE Trans. Geosci. Remote Sens.*, vol. 40, no. 4, pp. 793–800, Apr. 2002.

[34] V. N. Kudryavtsev, S. Fan, B. Zhang, A. A. Mouche, and B. Chapron, "On quad-polarized SAR measurements of the ocean surface," *IEEE Trans. Geosci. Remote Sens.*, vol. 57, no. 11, pp. 8362–8370, Nov. 2019.

[35] A. G. Voronovich and V. U. Zavorotny, "Theoretical model for scattering of radar signals in Ku- and C-bands from a rough sea surface with breaking waves," *Waves Random Media*, vol. 11, no. 3, pp. 247–269, Jul. 2001.

Gerardo Di Martino (Senior Member, IEEE) was born in Naples, Italy, in 1979. He received the Laurea degree (cum laude) in telecommunication engineering and the Ph.D. degree in electronic and telecommunication engineering from the University Federico II, Naples, in 2005 and 2009, respectively.

From 2009 to 2016, he was with the University of Naples Federico II, focusing on projects regarding applied electromagnetics and remote sensing topics. From 2014 to 2015, he was with the Italian National Consortium for Telecommunications (CNIT), Naples. In 2016, he joined the Regional Center Information Communication Technology (CeRICT), Naples. He is currently an Associate Professor of electromagnetics with the Department of Electrical Engineering and Information Technology, University of Naples Federico II. His research interests include microwave remote sensing and electromagnetics, with focus on electromagnetic scattering from natural surfaces and urban areas, synthetic aperture radar (SAR) signal processing and simulation, information retrieval from SAR data, and electromagnetic propagation in urban areas.

Prof. Di Martino is the Lead Associate Editor of the IEEE Geoscience and Remote Sensing Society Section within IEEE ACCESS. He is also an Associate Editor of the IEEE JOURNAL OF SELECTED TOPICS ON APPLIED EARTH OBSERVATIONS AND REMOTE SENSING, *Remote Sensing* (MDPI), and *Electronics* (MDPI).

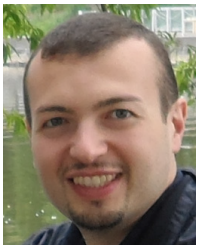

Alessio Di Simone (Member, IEEE) was born in Torre del Greco, Italy, in 1989. He received the B.Sc. and M.Sc. Laurea degrees (cum laude) in telecommunication engineering and the Ph.D. degree in information technology and electrical engineering from the University of Naples Federico II, Naples, Italy, in 2011, 2013, and 2017, respectively.

In 2016, he joined the Universitat Politècnica de Catalunya, Barcelona, Spain, as a Visiting Researcher. In 2017, 2018, and 2023, he was a Visiting Researcher with the NATO Science and Technology Organization, Centre for Maritime Research and Experimentation (CMRE), La Spezia, Italy. From 2017 to 2021, he was a Research Fellow with the Department of Electrical Engineering and Information Technology, University of Naples Federico II, where he has been an Assistant Professor of electromagnetic fields since 2022. His main research interests are in the field of microwave remote sensing and electromagnetics including modeling of the electromagnetic scattering from natural surfaces, urban areas, and artificial targets, and simulation and processing of synthetic aperture radar (SAR) and Global Navigation Satellite System Reflectometry (GNSS-R) data.

Dr. Di Simone received the Prize for the Best Master Thesis in Remote Sensing by the IEEE South Italy Geoscience and Remote Sensing Chapter in 2015 and the 2022 Best Young Researcher in Oceanic Engineering Award from the IEEE Oceanic Engineering Italy Chapter.

Antonio Iodice (Senior Member, IEEE) was born in Naples, Italy, in 1968. He received the Laurea degree (cum laude) in electronic engineering and the Ph.D. degree in electronic engineering and computer science from the University of Naples "Federico II," Naples, in 1993 and 1999, respectively.

In 1995, he joined the Research Institute for Electromagnetism and Electronic Components of the Italian National Council of Research (IRECE-CNR), Naples. From 1999 to 2000, he was with Telespazio S.p.A., Rome, Italy. He was with the University of Naples "Federico II" as a Research Scientist from 2000 to 2004 and as a Professor of electromagnetics from 2005 to 2018. He is currently a Full Professor of electromagnetics with the Department of Electrical Engineering and Information Technology, University of Naples "Federico II," where he is also the Coordinator of the B.S. and M.S. degree programs in Telecommunications and Digital Media Engineering. He has been involved as a Principal Investigator or a Co-Investigator in several projects funded by European Union (EU), Italian Space Agency (ASI), Italian Ministry of Education and Research (MIUR), Campania Regional Government, and private companies. He has authored or coauthored two books and more than 350 papers, of which over 100 published on refereed journals. His main research interests are in the field of microwave remote sensing and electromagnetics: modeling of electromagnetic scattering from natural surfaces and urban areas, simulation and processing of synthetic aperture radar (SAR) signals, and electromagnetic propagation in urban areas.

Prof. Iodice received the "2009 Sergei A. Schelkunoff Transactions Prize Paper Award" from the IEEE Antennas and Propagation Society, for the best paper published in 2008 on IEEE TRANSACTIONS ON ANTENNAS AND PROPAGATION. He was recognized by the IEEE Geoscience and Remote Sensing Society as a 2015 Best Reviewer of IEEE TRANSACTIONS ON GEOSCIENCE AND REMOTE SENSING. He is the Past Chair of the IEEE Geoscience and Remote Sensing South Italy Chapter.

Open Access funding provided by 'Università degli Studi di Napoli "Federico II"' within the CRUI CARE Agreement